Eur. J. Mech. B/Fluids

THREE-DIMENSIONAL EVOLUTION OF WIND WAVES FROM GRAVITY-CAPILLARY TO SHORT GRAVITY RANGE

G. Caulliez[1] and F. Collard

[1]: *Institut de Recherche sur les Phénomènes Hors Equilibre, Marseille, France. e-mail:* guil@pollux.irphe.univ-mrs.fr

(Received 25 October 1998, revised and accepted 23 January 1999)

Abstract – We report the first systematic laboratory observations of 3-D features of wind waves at early stages of wave field development. The experiments performed in the large IRPHE-Luminy wind-wave tank provided instantaneous reconstruction of the decimeter-scale water surface motions based on simultaneous imaging of the wave slopes in two perpendicular directions. Five essentially distinct regimes in the 3-D evolution of the dominant waves have been identified. Each regime is characterized by different types of 3-D wave patterns associated with specific ranges of wave scale and wave steepness. The likely scenario of the evolution and the possible physical mechanisms of the pattern formation are discussed. © Elsevier, Paris

1. Introduction

Three-dimensional features of wind-wave field developing at sea surface are indeed of principal importance for progress in the basic understanding of air-sea interaction processes and for remote sensing applications. This particular aspect of the wind-wave field evolution has been poorly studied yet inasmuch as the description provided by classical tools used in most observations, i.e. single-point measurements coupled with spectral analysis, is inadequate for getting such an insight. However, following the early works by Cox and Munk [4] and Stilwell [12] on analysis of sun glitter at the sea surface, the rapid development of high performance technology during the last decade, both in optics and data processing, has made realistic the use of optical imaging techniques to obtain a complete description of the 3-D properties of wind wave fields. Thus, stereo-photographic techniques have been recently developed for imaging large scale water surface motions at sea (Banner [1]; Shemdin et al [9]) while in laboratory, light refraction techniques have been used for spatial measurements of small-scale wave slopes in one or two perpendicular directions (Jähne and Riemer [6]; Zhang and Cox [14]). These investigations yielded a rather precise description of the two-dimensional wave slope spectra respectively near the dominant peak and at high wave numbers but were confined to a few wind and fetch conditions. Also, due to the relatively small size of wave slope-imaging systems used for observations, a first preliminary type analysis of the waveforms and the wave patterns shaping the water surface was conducted only for short capillary-gravity wind waves or parasitic capillaries generated by micro-breaking (Zhang [13]).

In this paper, we present a laboratory study carried out to investigate systematically the 3-D aspects of the evolution of the dominant wind waves propagated at the water surface at the early stages of wave field development, i.e. for waves from gravity-capillary to short gravity range. This study aims more specifically at characterizing the 3-D wave patterns which shape the water surface at the different stages of the wind wave evolution and then, at determining the conditions of their emergence as function of both the "external" parameters as wind speed or fetch and the "intrinsic" wave parameters as wavelength or wave steepness. Accordingly, the two-color visualization system developed to measure simultaneously both wave slope components over a large water surface area will be first described briefly. Then, the typical 3-D wave patterns to be associated

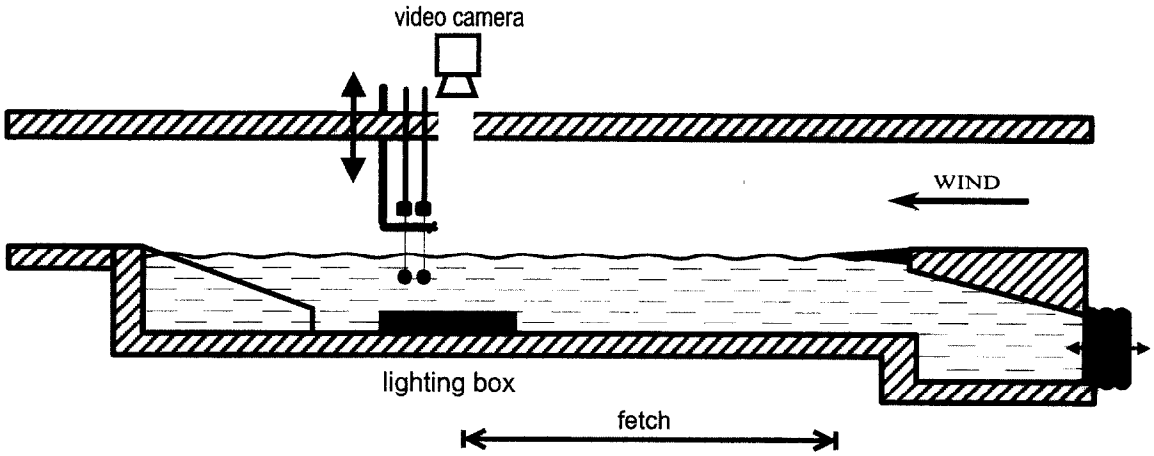

FIGURE 1. Schematic view of the large IRPHE wind-wave facility and the experimental arrangement used for imaging wave slopes at the water surface.

with different stages in the 3-D wind wave field evolution will be identified and investigated in more detail. The conditions for which the different regimes are observed as well as the basic wave parameters which control this evolution will be also specified. To conclude, a realistic scenario likely to describe the 3-D wave field evolution will be suggested.

2. The experimental procedure

The optical wave slope-measuring system adopted for wave visualization was based upon the method developed by Jähne and Riemer [6] which utilizes the light refraction at the water surface. The unique performance features of our system are first the ability to image the water surface slopes simultaneously in two perpendicular directions and second the large (compared to other installations) size of the spot allowing quality measurements. The essence of the system could be briefly discussed as follows. The light source is made of a square box (110 x 110 x 20 cm^3) illuminated from the downwind and crosswind side-walls by two long cylindrical luminescent tubes equipped with reflectors. The box contains an aqueous suspension of latex particles providing the scattering of the light in the box. A light source with two perpendicular gradients in brightness of two different colors is obtained by inserting two pass-band optical filters between the lamps and the scattering volume respectively. A 3-CCD video camera mounted at the top of the facility looking vertically downward allows to monitor the water surface motions. When waves are present at the water surface, the two-color images of the light source are directly modulated as a function of the two components of the wave slope. The latter at any point of the images are then derived by means of a simple ray tracing model. The special arrangement performed to increase the size of the images available for measurements is described in Shrira and Caulliez [11]. Here let us just mention that an image of size 85 x 85 cm^2 could be used for quantitative wave slope measurements for all wave conditions under consideration in this paper, with a relative error in slope less than 5%.

Wave observations were carried out in the large IRPHE wind-wave tank, 40 m long, 2.6 m wide and 1.0 m deep, as schematically shown in Fig. 1. Measurements of the water surface motions made by means of the wave slope imaging system described above and two capacitance wave gauges located at the immediate vicinity of the light box were complemented by measurements of the air surface flow structure using a set of velocity sensors (hot wires and Pitot tube). The wind speed will refer hereafter to the air potential flow velocity. The wave visualization system and the other measuring devices were set up at a fixed position in the water tank, at a distance of 28 m from the entrance, and the desired fetch was obtained by varying the length of the air-water junction plate. Special care was taken to ensure the uniformity of the wind at the entrance of the water tank

and the undisturbed development of the air surface boundary layer above the water surface. For this purpose a special flexible device was used to make smooth the transition between the solid wall at the edge of the air tunnel and the water surface. In these experiments, the wind and fetch conditions were chosen both to investigate the 3-D evolution of the dominant waves with fetch for several wind speeds and to observe waves of definite wavelength in various wind conditions.

For each condition, the images viewed by the video camera were digitized in real time by a RGB data acquisition board at intervals of 1 s and recorded directly on a PC computer. These images were coded into 256 x 350 pixels format (the longitudinal and transverse directions respectively) and 256 light intensity levels for each color channel. Then, for further analysis, the wave slope images were smoothed with a linear 2D low-pass filter of 2 pixels cut-off in scale in order to reduce the gaussian noise introduced by the data acquisition board at high wavenumbers (Jähne [5]). Average two-dimensional wavenumber slope spectra were computed from 100 independent images by means of a classical 2-D FFT algorithm after application of a Hanning window, and then remapped over a (k, θ) grid by means of a sub-grid algorithm. Integration of the spectra over the dominant peak provides too a direct estimation of the dominant wave steepness. To better identify the 3-D wave patterns, the instantaneous images of the water surface motions were also reconstructed from both slope images using an elaborated integration method (Kimmoun et al. [7]).

3. The experimental results

3.1. *The main stages of the evolution*

The qualitative investigations based on visual observations and photographs or by looking at the individual wave slope images have first shown that three-dimensional wave patterns are the dominant feature of the wind wave field at the early stages of development. The first quantitative results obtained by means of two-dimensional spectral analysis of the wave slope images then enabled us to distinguish five stages in the wind wave evolution depending on wavelength and wave steepness and directly associated with different 3-D coherent wave patterns. An illustration of the wave field features at these different stages is given in Figs. 2 where a side view of the wave field, an image of the water surface elevations reconstructed from wave slope images, and the contour lines of the 2-D wave slope spectra plotted both in a (k, θ) plan and in a sequence of constant-k plans, are displayed respectively for five typical wind and fetch conditions.

The *first stage* of the 3-D wind wave field evolution has been first detected by visual observations and photographs at relatively large fetches and very low wind speeds. As clearly seen in Fig. 2-1a, these wave motions shape the water surface into quite regular rhombic patterns resulting in a striking way from the growth of two quasi-monochromatic oblique waves. These waves correspond to the initial waves generated by wind in the tank for wind speeds below 4 m/s. They are observed at moderate to large fetches when the water surface still looks smooth. The (k, θ) wave slope spectrum shows that the wave field energy is mainly confined in a narrow band of wavenumbers independent on the wave propagation direction, but is distributed quite uniformly over a wide range of angles lying symmetrically on both sides of the wind direction (Figs. 2-1c and 2-1d). Although the images of the water surface motions show waves propagating roughly at $\pm$ 30° to the wind (Fig. 2-1b), no preferential angles could be seen in the spectra at this stage of evolution, looking practically flat from -30° to +30°. This peculiar shape of the spectra could be ascribed to the rather small signal to noise ratio observed in these conditions and related to the large time and space intermittence of the initial wind-generated waves propagating on the water surface as well-defined groups of few wavelengths or periods only. This intermittence is particularly noticeable in the time sequences of the water surface elevations observed in these conditions (Fig. 3a). The wavelength of these initial wind waves, is controlled by the wind speed and falls into range 4 to 10 cm. As it was shown previously (Ricci and Caulliez [8]), these wavelengths correspond to the scales of the most spatially-amplified wind waves at such light winds.

At wind speeds exceeding 4 m/s, the spatial growth of the initial wind waves at the entrance of the water tank becomes very rapid and the domain corresponding to the growth of the initial wind waves is localized in the first meter of the tank, just downwind of the air-water junction plate. The characteristic scales of the

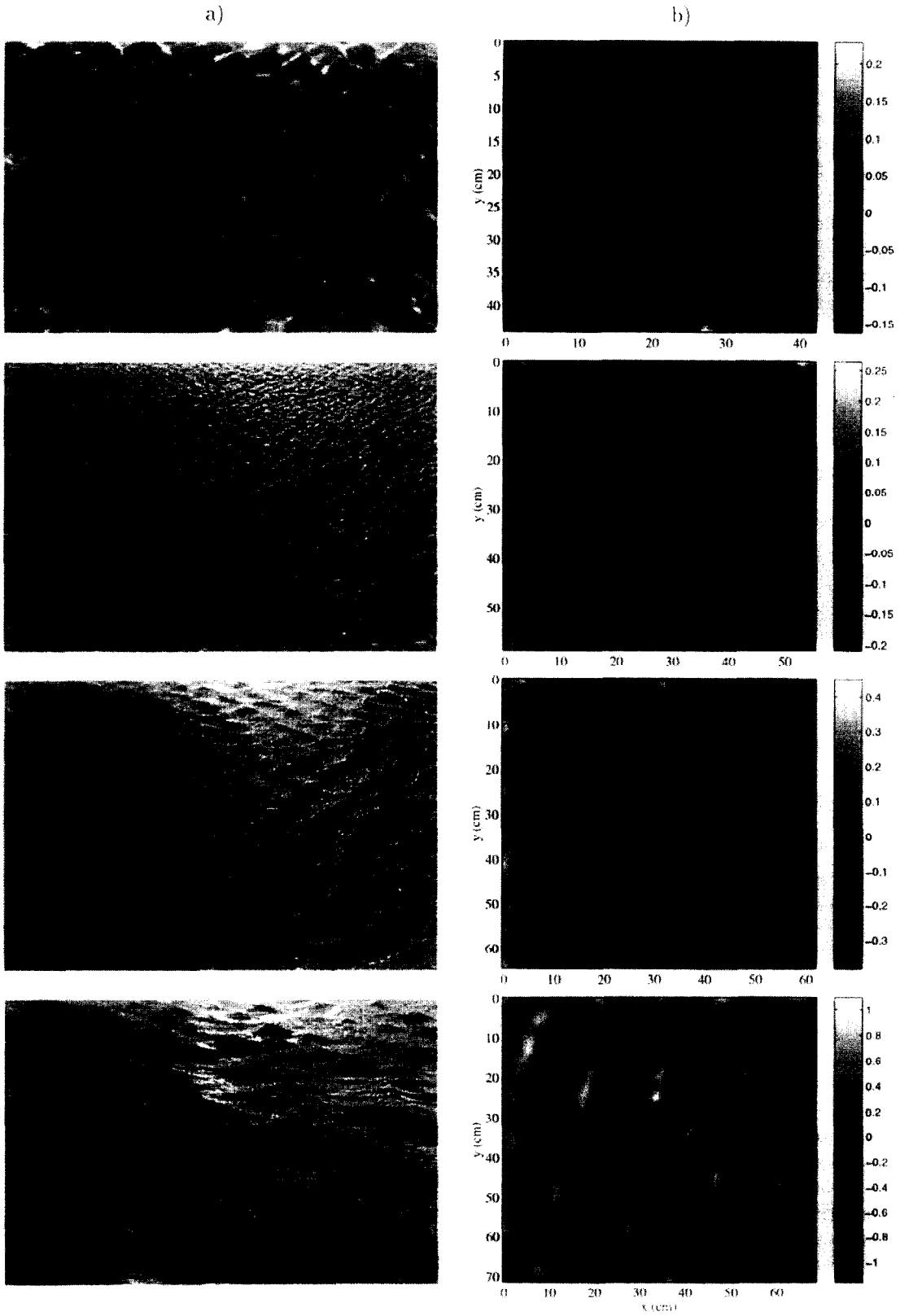
a)
b)
y (cm)
0
5
10
15
20
25
30
35
40
0
10
20
30
40
0.2
0.15
0.1
0.05
0
−0.05
−0.1
−0.15
y (cm)
0
10
20
30
40
50
0
10
20
30
40
50
0.25
0.2
0.15
0.1
0.05
0
−0.05
−0.1
−0.15
−0.2
y (cm)
0
10
20
30
40
50
60
0
10
20
30
40
50
60
0.4
0.3
0.2
0.1
0
−0.1
−0.2
−0.3
y (cm)
0
10
20
30
40
50
60
70
0
10
20
30
40
50
60
1
0.8
0.6
0.4
0.2
0
−0.2
−0.4
−0.6
−0.8
−1

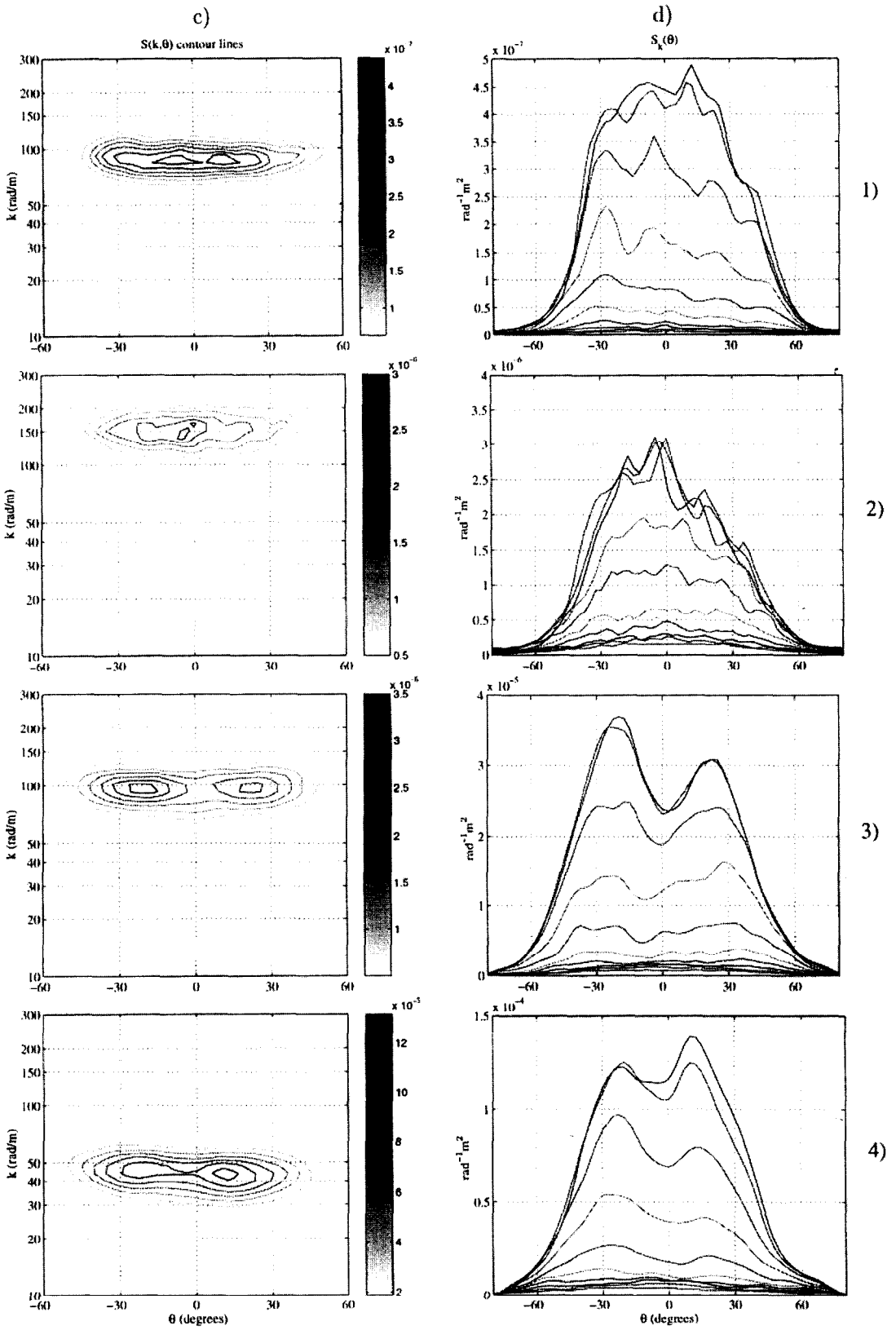
c)
d)
S(k,θ) contour lines
$S_k(\theta)$
k (rad/m)
θ (degrees)
rad^{-1}m^2
1)
2)
3)
4)

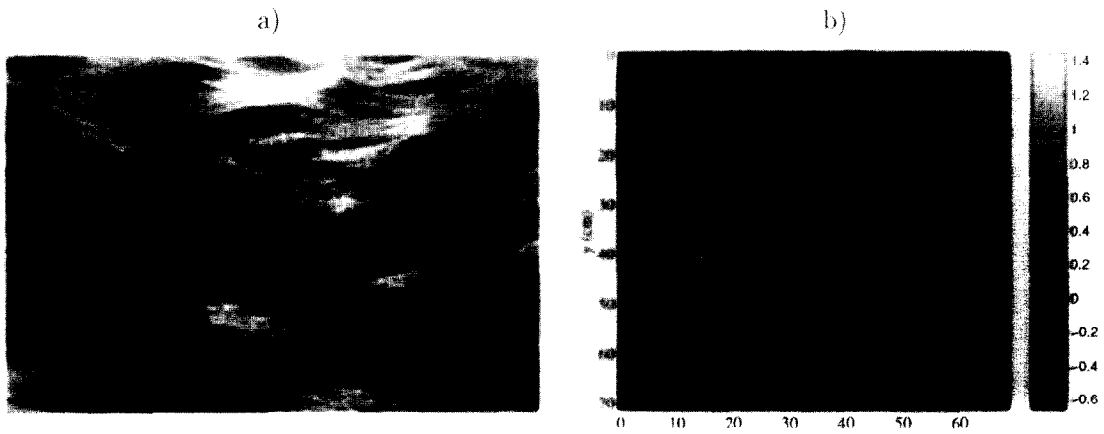

FIGURE 2 : see the facing page

most amplified wind waves decrease sharply as well, reaching values smaller than 4 cm in wavelength. At this stage of development (called stage "0" hereafter), the visual observations suggest that the 3-D character of the initial waves is not so well-pronounced. However, the wave field displays there a great inhomogeneity of the order of the wave scales themselves, caused by the laminar-turbulent transition of the drift current (Caulliez et al. [3]). Therefore, quantitative wave slope measurements are difficult to make and especially to interpret in such conditions.

The *second stage* of the 3-D wave evolution was observed at wind speeds higher than 4 m/s when the initial wind waves fully develop, i.e. just before the start of the frequency and wavenumber downshift phenomenon (i.e. the decrease with fetch of the dominant wave frequency and wavenumber). As illustrated in Figs. 2-2a and 2-2b, the water surface, looking uniformly rough is entirely ruffled by small-scale capillary-gravity waves of high steepness. These waves are shaped with typical round crests and sharp troughs. The random distribution in space of such short-crested waves, quite noticeable just by looking by unaided eye at the water surface, is reflected in the shape of the wave slope spectra, which are of significant broadness both in k and θ (Fig. 2-2c). At this stage of evolution, the angular distribution of the spectral energy density at the dominant wavenumber is maximal for the along-wind direction, but still remains wide, $S_k(\theta)$ keeping large values for angles up to $\pm$ 30° (Fig. 2-2d).

The *third stage* of the 3-D evolution of the wind waves concerns waves of scales similar to the initial waves observed at very low wind speeds (stage I). As shown in Fig. 2-3a, the wave field exhibits noticeable 3-D wave patterns as well, but surprisingly, these rhombic patterns emerge gradually out of the random short capillary-gravity wave field described above (stage II). This phenomenon occurs when the dominant wavelength starts to increase. In a very similar way, the 3-D patterns are formed by two symmetric oblique waves propagating at angles close to $\pm$ 30° to the wind direction (Fig. 2-3b). The gravity-capillary wave profiles of significant steepness here are distorted by conspicuous trains of capillary waves localized on the forward face of the crests. The wave slope spectra then display two well-pronounced peaks centered more or less symmetrically at about $\pm$ 25° (Figs. 2-3c and 2-3d). The existence of such distinguishable peaks suggests essentially coherent nature of the 3-D wave patterns observed at this stage of development.

For wind speeds exceeding 4 m/s the next, i.e. the *fourth, stage* of wind wave evolution corresponds to the development of steep short-crested gravity waves of wavelength ranging approximately between 10 and 20 cm, as shown in Figs. 2-4a and 2-4b. This stage occurs in a well-defined range of fetches specified by the wind speed. The wave field exhibits rather regular and well-pronounced 3-D patterns shaping the water surface as rhombi, pentagons or hexagons, but the length and the orientation of the ridges forming the 3-D patterns varies widely in space. In fact, the configuration of the patterns looks dependent on the local steepness which changes significantly both in space and time due to the persistence of well-pronounced wave groups

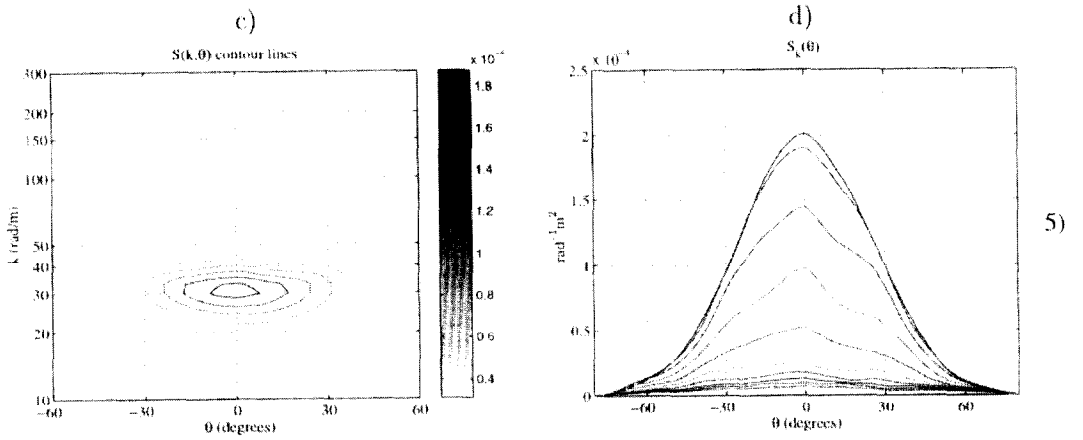

FIGURE 2. Illustration of the wind wave features at the five stages of the 3-d evolution:
1) stage I (U = 2.5 m/s; X = 26 m); 2) stage II (U = 6 m/s, X = 2 m); 3) stage III (U = 5 m/s, X = 6 m); 4) stage IV (U = 6 m/s, X = 9 m); 5) stage V (U = 5 m/s, X = 18 m);
a) Side view of the wind wave field, with the wind blowing from right to left;
b) Image of the water surface elevations (scale in cm) obtained by reconstruction from both wave slope images, with the wind blowing from right to left;
c) Contour lines of the (k, θ) wave slope spectrum for the different energy levels indicated in the right scale (scale in m^2 rad^{-1});
d) Contour lines of the (k, θ) wave slope spectrum in the succession of constant-k plans k_i = (1 + 0.1 i) k_{peak} with k_{peak} = 83.5, 137, 92, 43, 30 rad/m respectively and $i = 0, 1, 2, ..., 9$.

(Fig. 3d). In particular, it seems that the occurrence of the first micro-breakings would be at the origin of the pentagon pattern formation (such a pattern is particularly well visible in Fig. 2-5b). To a certain extent, these various features give to the wave field a random and rather rough aspect. However, two peaks can be easily distinguished in the two-dimensional wavenumber spectra of the wave slope images (Figs. 2-4c and 2-4d), indicating the coherency of the 3-D wave patterns is still large there. Note that for such longer waves, the peaks are found at smaller angles, about ± 20° or less, and are generally less symmetric.

The last, *fifth, stage* of the 3-D evolution of the wave field occurs when the dominant waves reach a certain energy equilibrium resulting from the balance between the wind input to wave motions and the wave dissipation due to breaking or micro-breaking and nonlinear transfer to larger scales. This stage is observed for short gravity waves of wavelength as small as 12 cm at low wind speeds, but longer than 25 cm for the highest wind speeds. The wave field is then composed both of short-crested waves and long-crested waves distributed randomly and forming intermittent 3-D wave patterns of different shape at the water surface (Figs. 2-5a and 2-5b). The 3-D aspect of the wave field is also emphasized by the existence of small-scale wavetrains generated by micro-breaking waves or crescent-shaped breaking waves and propagating in transverse direction to the wind. This noticeable evolution of the wave field 3-D features is well depicted by the drastic change in the shape of the wave slope (k, θ) spectra (Figs. 2-5c and 2-5d). The latter exhibit now only one smooth peak at the dominant wave number, centered at zero angle. Compared to the individual peaks observed previously, this peak is broader in k and θ. This corroborates the large variability in scale, in shape and in wave direction of the dominant waves at this stage of evolution.

3.2. *The main characteristics of the dominant waves*

To better specify the wave parameters which control the 3-D wave field evolution described above and then to attempt to determine the physical processes involved, a detailed analysis of the mean dominant wave features has been performed for the whole set of experiments. As this has never been described before in such a large

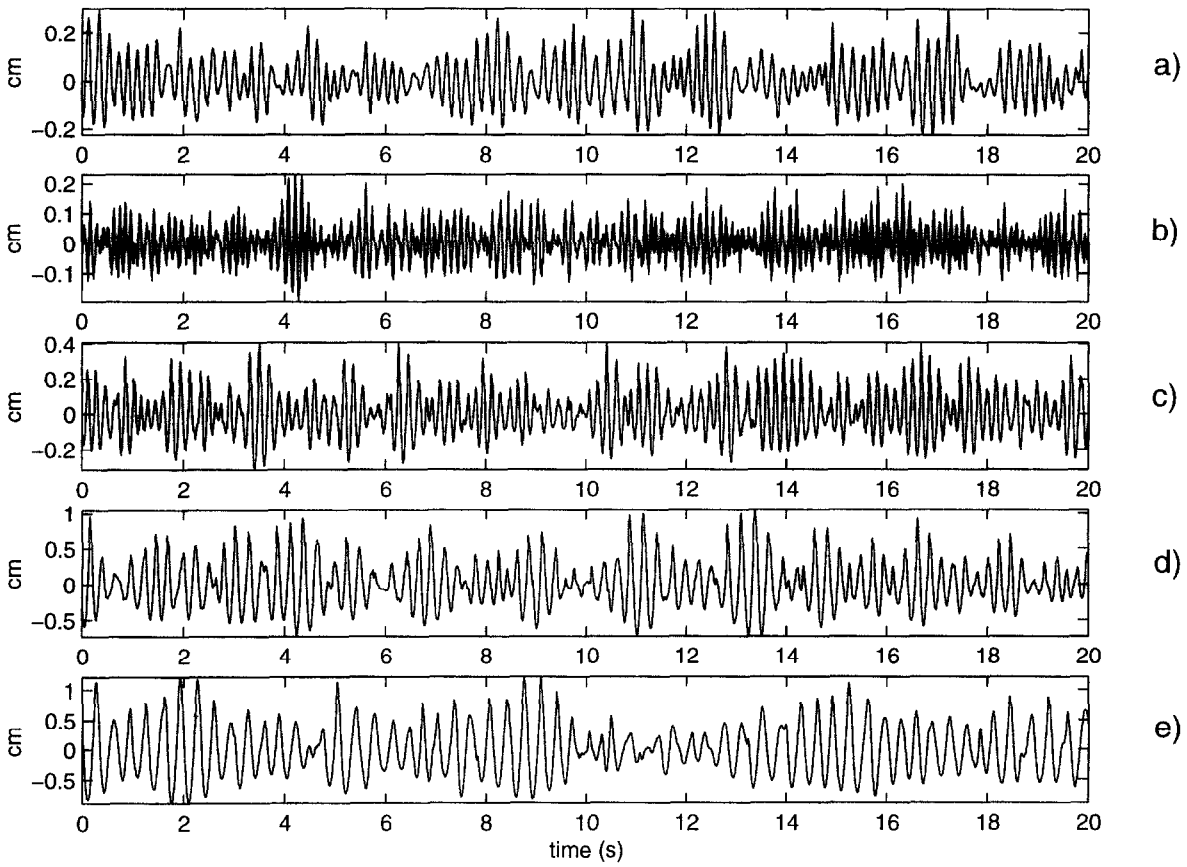

FIGURE 3. Time series of the water surface elevations measured by a capacitance wave gauge set up at the immediate vicinity of the light box for different wind and fetch conditions characteristic of the five stages of the 3-D wave field evolution: a): U = 2.5 m/s, X = 26 m (stage I) ; b): U = 6.0 m/s, X = 2 m (stage II) ; c): U = 5.0 m/s, X = 6 m (stage III) ; d): U = 6.0 m/s, X = 9 m (stage IV) ; e): U = 5.0 m/s, X = 18 m (stage V) .

wind-wave tank due to the lack of appropriate measuring techniques, the parallel evolution of the wavelength and the wave steepness of the dominant waves was investigated as function of fetch and wind speed (Figs. 4 and 5). First, these results highlight that the wavelength increases only slowly with fetch when the dominant waves lie in the gravity-capillary domain ($\lambda \leq 8$ cm). However, for short gravity waves this growth enhances rapidly, fitting remarkably linear dependence on fetch of slope increasing with wind. The evolution of the wave steepness with fetch confirms that the wave field reaches rapidly a kind of dynamical equilibrium at larger fetches whatever the wind conditions, except for the lowest wind speed (2.5 m/s), where a significant steepness increase may hold at 26 m fetch. Note the fact, that at large fetches the linear increase of the dominant wavelength is not affected by the occurrence of the wave energy saturation.

The spectral analysis made above shows very clearly that at a given wind and fetch condition, the wavenumber of the dominant waves does not vary with the wave propagation direction, and this holds whatever the conditions. Therefore, the mean 3-D features of the dominant waves are better described by the angular distribution function $Y(\theta)$ obtained by the integration of the spectral energy density of the wave slopes over the dominant peak k-domain. The simplest single quantity to characterize this distribution is the angular dispersion defined here as the average angle at which $Y(\theta)$ reaches half of its maximum value. This parameter is found to be higher than

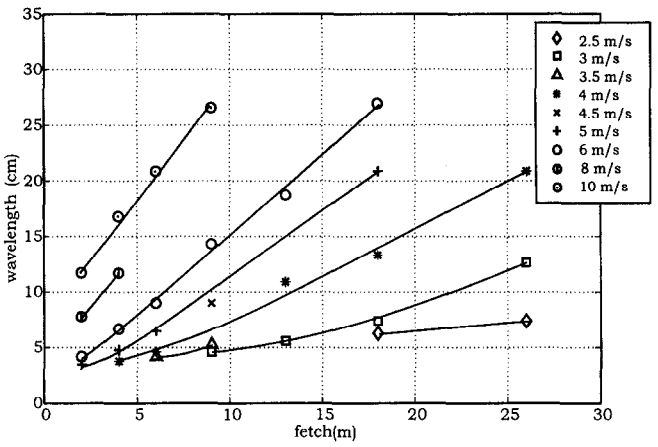

FIGURE 4. Evolution with fetch of the dominant wavelength observed in the large IRPHE wind-wave tank for the various wind conditions investigated.

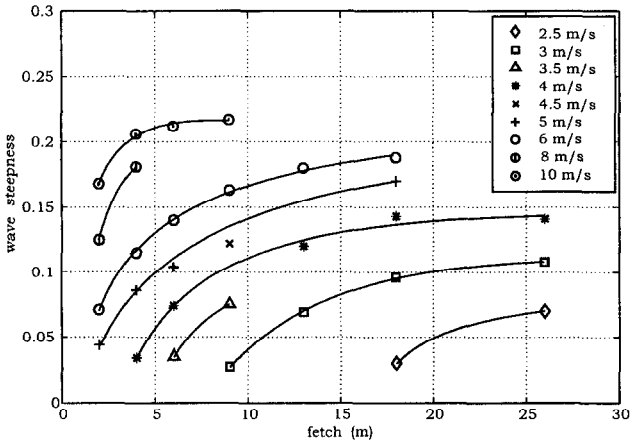

FIGURE 5. Evolution with fetch of the dominant wave steepness observed in the large IRPHE wind-wave tank for the various wind conditions investigated.

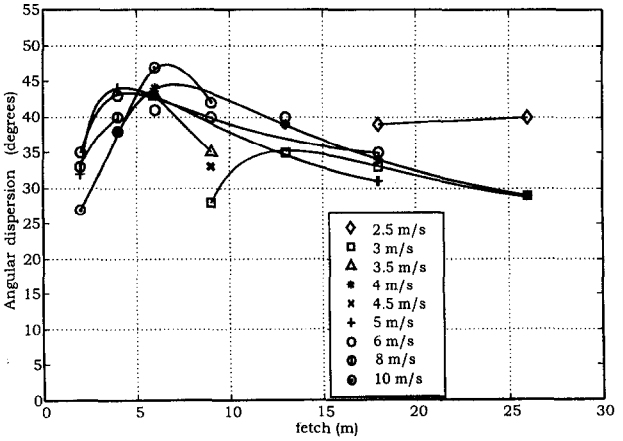

FIGURE 6. Evolution with fetch of the angular dispersion of the dominant waves observed in the large IRPHE wind-wave tank for the various wind conditions investigated.

30° for the most of the experimental conditions we investigated with a maximum close to 45° at the intermediate fetches (Fig. 6). The highest values of the angular dispersion concern the gravity-capillary waves of wavelength 4 to 10 cm observed at small to moderate wind speeds.

As just inferred above but clearly shown in Figs. 7a-d, the shape of the dominant wave angular distribution shows large similarities for waves of comparable wavelength but measured in different experimental conditions. In particular, the gravity-capillary waves of 4 cm wavelength or less observed at stage II are characterized by a wide and round-shaped curve centered approximately in the wind direction (Fig. 7a). Such a distribution has to be associated with the typical random and short-crested aspect of the small-scale waves developing at the water surface. On the contrary, the angular distribution of the relatively 'long' gravity-capillary waves in the wavelength range 4 - 10 cm observed both in stages I and III is practically flat within the angle sector of approximately ± 30° when the wave steepness is small at low wind speeds (Fig. 7b). When the wave steepness is higher ($ak \geq 0.08$), the angular distribution exhibits two well-pronounced peaks located at two symmetric angles close to ± 30°. In this case, the short-crested character of the wave field is due to two oblique wavetrains propagating at about ± 30° to the wind direction and forming relatively regular rhombic patterns at the water surface. For short gravity waves of wavelengths in the range approximately 10 to 20 cm observed at stage IV the angular distribution still exhibits two peaks, but the particular shape of this function, such as the peak sharpness and the peak separation, is controlled by the combined evolution of the wavelength and the wave steepness (Fig. 7c). At the last stage of development when the wave field reaches an equilibrium characterized by the saturation of the wave steepness growth with fetch (stage V), the shape of the angular distribution of the short gravity waves changes completely (Fig. 7d). This function displays now only one smooth peak centered approximately at zero angle, indicating that these wind waves with intermittent long crests mainly propagate at small angles to wind.

These results corroborate undoubtedly the existence of five essentially distinct stages in the 3-D evolution of the wave field generated by wind at limited fetches, as displayed in Fig. 8. Furthermore, they indicate that the parameters which control this evolution, and, consequently, the balance between the different processes responsible for energy transfer to dominant waves, are mainly related to the wave scale and to a less extent to the wave steepness.

This analysis then enables us to determine rather precisely the ranges of wavelength and wave steepness to be associated with these five stages of evolution (Fig. 9). However, it should be mentioned that the boundaries of domains are not sharp and are, in fact, smooth transitions from one stage to the other. Note that it is likely that these boundaries might be slightly modified by a change in an external parameter of secondary importance for the wave development, as, for instance, the drift current development or the air flow turbulence.

The main features of the dominant wave field which characterize the different stages of the three-dimensional evolution are also summarized in Table 1. The table is effectively splitted into two: the upper one is for winds below 4 m/s, while the lower one is for wind exceeding this threshold. There is qualitative difference between the two cases: in the former case, no waves of wavelength smaller than 4 cm can be generated by wind as the wind input is not high enough to allow the growth of short gravity waves of significant steepness before the energy saturation.

4. Discussion and conclusion

The most striking aspects of the three-dimensional evolution of the wind wave field we have described above lie essentially in:

i) the generation at very low wind speed (U < 4 m/s) of two oblique waves propagating symmetrically at ± 30° to the wind. These motions observed at stage I correspond to the initial waves generated by wind at the water surface;

ii) the development at higher wind speeds of two oblique waves propagating at angles close to ± 30° to the wind direction which emerge from a well-developed but randomly-distributed capillary-gravity wave field of shorter scales, that characterizes the stage III.

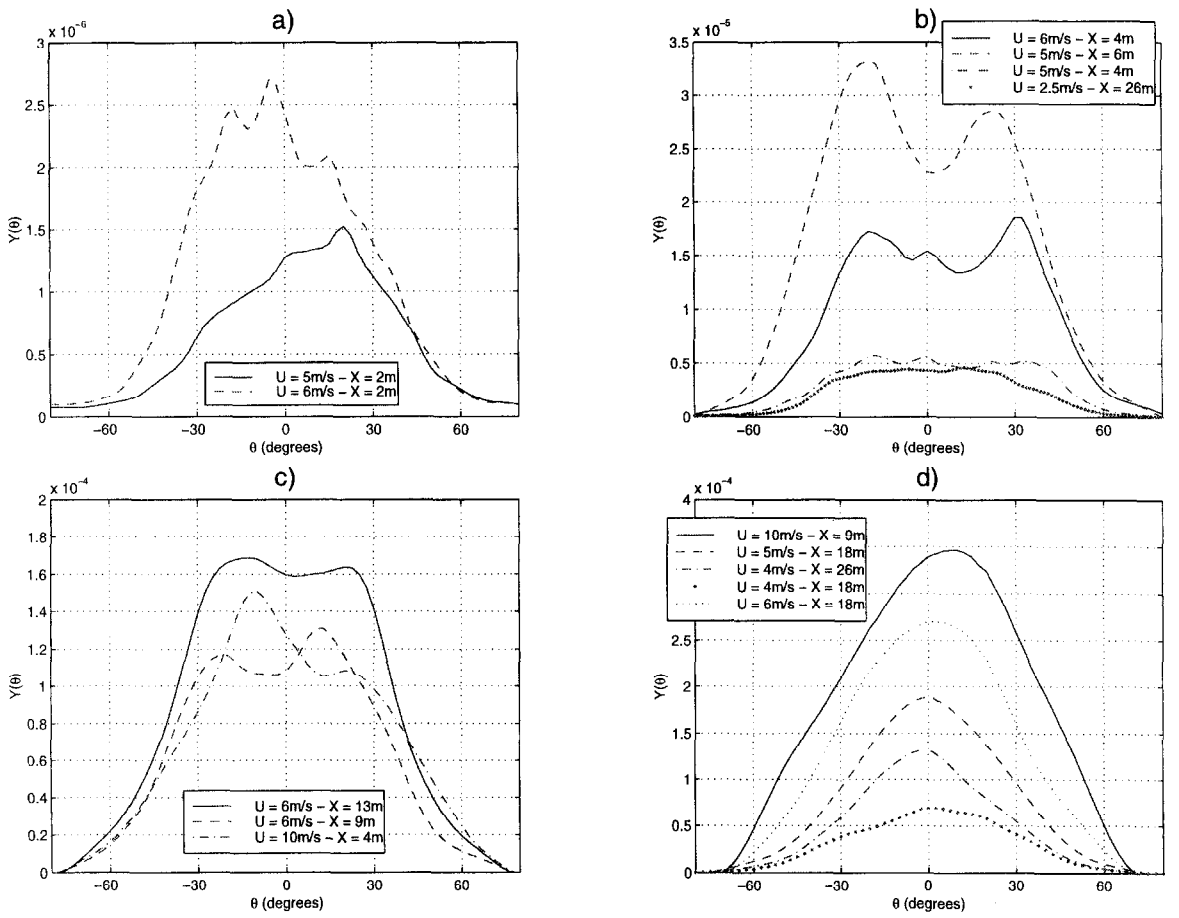

FIGURE 7. Angular energy distribution of the dominant waves $Y(\theta)$ estimated from the wave slope images for various wind and fetch conditions characteristic of the five stages of the 3-d wind wave field evolution (λ is given for the lowest to highest curves):
a) stage II ($\lambda = 3.5$ cm; $\lambda = 4.2$ cm),
b) stage I and stage III ($\lambda = 7.4$ cm; $\lambda = 4.6$ cm; $\lambda = 6.7$ cm; $\lambda = 6.5$ cm),
c) stage IV ($\lambda = 11.7$ cm; $\lambda = 14.3$ cm; $\lambda = 18.7$ cm),
d) stage V ($\lambda = 13.3$ cm; $\lambda = 20.9$ cm; $\lambda = 20.9$ cm; $\lambda = 27.0$ cm, $\lambda = 26.6$ cm).

In both cases, these wave motions form rhombic patterns of similar shape at the water surface, although their wave steepness can differ by the factor of 3 or 4. Their wavelength falls into a very specific range of scales, namely, between 4 and 10 cm, and then belongs entirely to the gravitational branch of the gravity-capillary wave k-domain located just below the minimum of the phase velocity even if accounted for the correction due to the current. Their typical angular energy distribution is rather flat at low steepness but strictly bimodal at higher steepness, and, most remarkably, without any distinguishable component in the along-wind direction (Fig. 7b).

Let us examine the possible mechanisms of formation of these well-pronounced 3-D wave patterns. First, the particular conditions of emergence of such 3-D wave patterns of definite scales suggest immediately that some resonant wave-wave interaction processes may be at their origin. However, it is well-known that resonant triad interaction processes can lead to the formation of oblique waves from disturbances generated by wind in the along-wind direction for waves belonging to the capillary branch of the capillary-gravity waves. When the

	regime	type of waves	λ (cm)	ak fetch evol	$Y(\theta)$	θ_{peak}
U < 4 m/s	I	initial smooth capillary-gravity waves	4 - 10	increase	flat	-30° to +30°
	V	random long-crested gravity waves	> 10	saturation	1 peak	≈ 0°
	Ib	initial wind-generated capillary-gravity waves	< 4	≈ 0.01		
U > 4 m/s	II	short capillary-gravity waves of rough aspect	< 4	increase	1 peak	≈ 0°
	III	two oblique "long" capillary-gravity waves	4 - 10	increase	2 peaks	± 30°
	IV	steep short-crested gravity waves	> 10	> 0.12 increase	2 peaks	[0°, ± 30°]
	V	random long- and short-crested gravity waves	> 12	saturation	1 peak	≈ 0°

TABLE 1

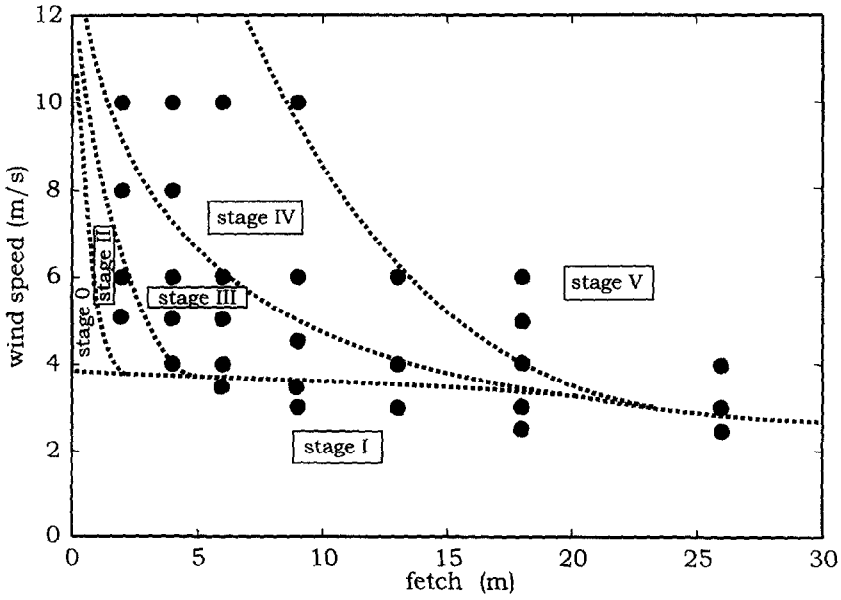

FIGURE 8. Schematic diagram showing the respective domains in wind speed and fetch associated with the different stages of the 3-D wind wave field evolution observed in the large IRPHE wind-wave facility (the symbols indicate the different wind and fetch conditions investigated).

effect of the drift current on the dispersion relation is taken into account, these waves prove to be of scales no longer than 5 cm (Shrira and Caulliez [11]). Thus, such process which may occur in cascade would be rather the best candidate to explain the formation of the 3-D wave field of rough aspect observed at stage II. Second, the nonlinear wave-current interactions have to be also considered in the context of this work. These processes are essentially of the same nature as those responsible for the generation of Langmuir circulations inside the upper water shear layer but due to the feedback of water circulations on surface waves, they lead to the formation of

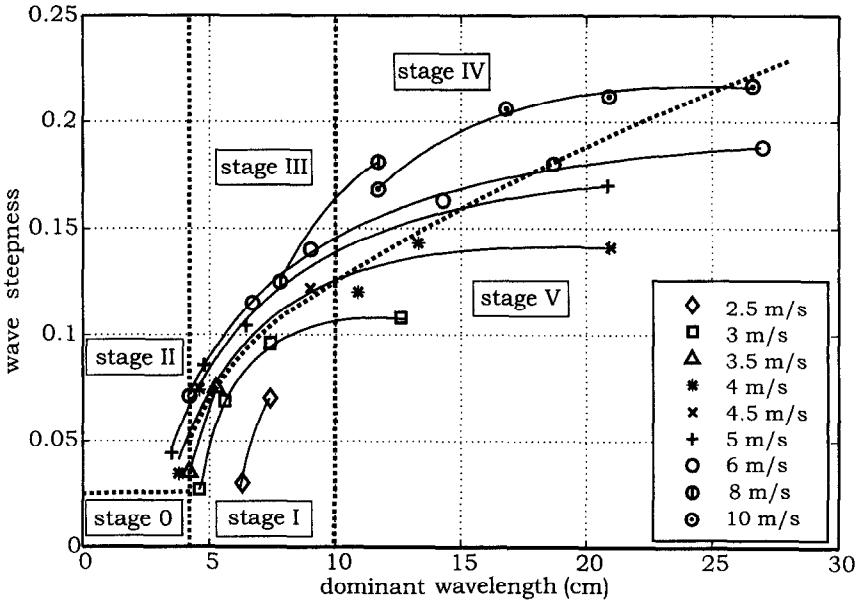

FIGURE 9. Evolution with the dominant wavelength of the dominant wave steepness observed for the various wind conditions investigated. The dashed bold lines indicate the limits in wavelength and wave steepness of the different stages of the 3-D wind wave field evolution.

short-crested waves (Shrira [10]). However, we found from previous observations that the growth of the 3-D initial waves observed at stage I is associated with the development of a laminar-turbulent transition in the drift current (Caulliez et al. [3]). In addition, visualizations have shown that the development of Langmuir-like circulations in water occurs only for higher wind speeds and shorter fetches. Such results would discard a priori this nonlinear wave-current interaction process as the main mechanism responsible directly for the 3-D wave pattern formation at stage I of evolution, as very likely at stage III.

The above considerations suggest, that the emergence of two oblique waves in the range of wavelengths from 4 to 10 cm should be rather searched into the development of some nonlinear wave-wave interactions specific for this range of scales. The existence of such a selective mechanism, not investigated or not even clearly identified yet, would be strongly supported by the very sharp decrease of the angular energy distribution observed for the angles larger than those of the peaks (see Fig. 7b).

The next stage in the 3-D evolution of the wave field is characterized by the formation of steep short-crested gravity waves as found at larger fetches (stage IV). These still steepening waves, of wavelengths between 10 cm and 20 cm, develop only at moderate to high wind speeds. The wave angular energy distribution exhibits two peaks, but the distance between the peaks decreases gradually. The rate of decrease accelerates with slowing down of the wave steepness growth. Finally, the last stage of 3-D wave evolution (stage V) was found associated with the energy saturation of the wave field. At this stage, the dominant wavelength still increases, whereas the wave steepness growth practically stops. Simultaneously, the shape of the 3-D patterns becomes more variable, associated both with long-crested and short-crested waves propagating in random directions at small angles to the wind. The wave field is characterized by an angular energy distribution exhibiting only one central peak.

The coupled evolution with wind and fetch of the wavelength, the wave steepness and the angular dispersion of the waves observed both in stage IV and in stage V suggests that the development of the wave field is controlled there by the competition between two phenomena:

i) the wind which tends to amplify the dominant waves or smaller-scale disturbances in the along-wind direction at a higher rate, through linear or nonlinear instability mechanisms (Belcher [2] and personal communication);

ii) an yet to be identified nonlinear wave-wave or wave-current interaction mechanism which redistributes the

wave energy over a broader angular spectrum. The efficiency of such process would depend directly on the wave steepness growth, that constitutes a peculiarity of interest for further understanding.

To conclude, the whole set of the findings and considerations given above enables us to suggest a specific scenario to describe the 3-D evolution of the wind wave field at the early stages of wave development. First, the whole 3-D evolution of the wind wave field appears essentially controlled by the emergence at short fetches of two oblique waves, of wavelengths in the range 4 to 10 cm, propagating at about $\pm$ 30° to the wind direction and forming quite regular rhombic patterns at the water surface. This regime would originate from the development of some nonlinear wave-wave interaction mechanism specific to this range of scale. Further investigations are carried on now to identify this mechanism more precisely. Then, when the dominant wavelength moves to short gravity domain, the wave field preserves for high enough wind speed a well-pronounced 3-D feature characterized both qualitatively, by its short-crested aspect and quantitatively, by a bimodal angular energy distribution. This regime occurs as long as the wave steepness increases significantly. It would be the result of opposing action of the intense wind forcing which causes simultaneously a higher growth of the wave disturbances in the along-wind direction with a large steepness increase, the latter keeping the nonlinear wave-wave interaction processes very effective. At last, when the energy saturation is reached, the wave motions relax to a broad-band angular spectrum wave field of random aspect. Its 3-D feature would be the result of a rather complex interplay between the wind action and the nonlinear wave-wave and wave-current interactions.

Acknowledgements

We would like to express sincere thanks to V. Shrira for the helpful discussions we shared during the course of this work and his valuable comments on the first draft of the manuscript. We gratefully acknowledge US ONR for financial support under grant N-00014-94-1-0532.

References

[1] Banner M.L., Jones I.S.F., Trinder J.C., 1989, Wavenumber spectra of short gravity waves, J. Fluid Mech. 198, 321-344.
[2] Belcher S. E., 1999, Wave growth by non-separated sheltering, Eur. J. Mech. B/Fluids this issue, 121-136.
[3] Caulliez G., Ricci N., Dupont R., 1998, The generation of the first visible wind waves, Phys. Fluids 10, 4, 757-759.
[4] Cox C., Munk W.H., 1954, Statistics of the sea surface derived from sun glitter, J. Marine Res. 13, 2, 198-227.
[5] Jähne B., 1993, Digital Image Processing: Concepts, Algorithms and Scientific Applications., Springer-Verlag, Berlin.
[6] Jähne B., Riemer K.S., 1990, Two-dimensional wave number spectra of small-scale water surface waves, J. Geophys. Res. 95, 11531-546.
[7] Kimmoun O., Branger H., Kharif C. 1999, On short-crested waves: experimental and analytical investigations, Eur. J. Mech. B/Fluids (to appear).
[8] Ricci N., Caulliez G., 1994, Characteristic scales of the initial wind-generated waves, C. R. Acad. Sci. Paris II 318, 1591-1598.
[9] Shemdin O.H., Tran H.M., Wu S.C., 1988, Directional measurements of short ocean waves with stereophotography, J. Geophys. Res. 93, 13891-901.
[10] Shrira V.I., 1998, Wind wave nonlinear interactions owing to drift current: formation of the angular spectrum, wave groups and Langmuir circulations, in: Perrie (ed), Nonlinear Ocean Waves, Computational Mechanics Publications, Southampton, 163-206.
[11] Shrira V., Caulliez G., 1998, Three-dimensional water wave patterns in gravity and gravity-capillary range, O.N.R. report.
[12] Stilwell D. J., 1969, Directional energy spectra of the sea from photographs, J. Geophys. Res. 74, 8, 1974-1986.
[13] Zhang X., 1995, Capillary-gravity and capillary waves generated in a wind wave tank: observations and theories, J. Fluid Mech. 289, 51-82.
[14] Zhang X, Cox C.S., 1994, Measuring the two dimensional structure of a wavy water surface optically: a surface gradient detector, Exp. Fluids 17, 225-237.